Journal of Power Sources 245 (2014) 37–47

Contents lists available at SciVerse ScienceDirect

Journal of Power Sources

journal homepage: www.elsevier.com/locate/jpowsour

Improvement in direct methanol fuel cell performance by treating the anode at high anodic potential

Prabhuram Joghee [a,*], Svitlana Pylypenko [a,b], Kevin Wood [a], April Corpuz [c], Guido Bender [b], Huyen N. Dinh [b], Ryan O'Hayre [a]

[a] Colorado School of Mines, Department of Metallurgical & Materials Engineering, 1500 Illinois St., Golden, CO 80401, United States
[b] National Renewable Energy Laboratory, 1617 Cole Boulevard, Golden, CO 80401, United States
[c] Department of Chemical and Biological Engineering, University of Colorado Boulder, UCB 596, Boulder, CO 80303, United States

HIGHLIGHTS

- Anodic treatment (AT) at 0.8 V vs. DHE for DMFC anodes containing PtRu/C has been investigated.
- A significant improvement in DMFC performance has been observed after AT.
- It is demonstrated that reorganization of the Nafion ionomer takes place in the anode catalyst layer during AT.
- AT could be used as an additional break-in protocol in DMFC along with conventional protocols to enhance performance.

ARTICLE INFO

Article history:
Received 12 February 2013
Received in revised form
2 May 2013
Accepted 18 June 2013
Available online 27 June 2013

Keywords:
Direct methanol fuel cell
Anodic treatment
MOR polarization
Long-term performance
CO stripping voltammetry
Reorganization of Nafion ionomer

ABSTRACT

This work investigates the effect of a high anodic potential treatment protocol on the performance of a direct methanol fuel cell (DMFC). DMFC membrane electrode assemblies (MEAs) with PtRu/C (Hi-spec 5000) anode catalyst are subjected to anodic treatment (AT) at 0.8 V vs. DHE using potentiostatic method. Despite causing a slight decrease in the electrochemical surface area (ECSA) of the anode, associated with ruthenium dissolution, AT results in significant improvement in DMFC performance in the ohmic and mass transfer regions and increases the maximum power density by ~15%. Furthermore, AT improves the long-term DMFC stability by reducing the degradation of the anode catalyst. From XPS investigation, it is hypothesized that the improved performance of AT-treated MEAs is related to an improved interface between the catalyst and Nafion ionomer. Among potential explanations, this improvement may be caused by incorporation of the ionomer within the secondary pores of PtRu/C agglomerates, which generates a percolating network of ionomer between PtRu/C agglomerates in the catalyst layer. Furthermore, the decreased concentration of hydrophobic CF_2 groups may help to enhance the hydrophilicity of the catalyst layer, thereby increasing the accessibility of methanol and resulting in better performance in the high current density region.

1. Introduction

The direct methanol fuel cell (DMFC) is a potential alternative power source for a number of applications, including portable electronic devices [1,2]. However, the initial and long-term performance of DMFCs remains insufficient for commercial applications. This is mainly attributed to poor electro-catalytic activity of the state-of-the-art PtRu catalysts employed for the methanol oxidation reaction (MOR) in the anode [3,4], as well as time-dependent performance loss factors. These factors include methanol crossover from anode to cathode [5–7], Ru dissolution and migration to cathode [8–10], and interfacial de-lamination within the membrane electrode assembly (MEA) during long-term operation [11,12]. The poor electro-catalytic activity of most PtRu catalysts can be at least partly attributed to non-optimized utilization of PtRu in the anode due to inadequate break-in of the MEA [13,14].

In the literature, several MEA break-in methods have been suggested in order to increase the utilization of PtRu (anode) and Pt (cathode) catalysts, respectively [13–18]. He et al. [14] demonstrated improved DMFC performance and improved utilization of anode (PtRu) and cathode (Pt) catalysts after a break-in procedure which involved subjecting the cell to H_2 evolution by an

* Corresponding author. Tel.: +1 720 216 3898, +1 303 273 3057.
E-mail addresses: pjoghee@mines.edu, prabhu2166@yahoo.com (P. Joghee).

0378-7753/$ – see front matter © 2013 Elsevier B.V. All rights reserved.
http://dx.doi.org/10.1016/j.jpowsour.2013.06.105

electrochemical method. Inoue et al. [13] introduced a two-step protocol to break-in DMFC MEAs to increase performance. The initial break-in was accomplished using H_2/O_2 (i.e. under hydrogen fuel cell mode) at a constant voltage at 0.21 V for 3 h; subsequently, a conventional methanol/O_2 break-in was conducted for further 27 h. This two-step break-in procedure increased initial DMFC performance by ~34% as compared against an identical MEA that was subjected to a conventional methanol/O_2 break-in procedure only. In other studies, an improvement in DMFC performance has been observed after pre-treating an MEA with water or methanol solution prior to performance testing [15,17]. For example, an MEA pretreated with methanol solution maintained ~100 mV higher potential at 70 mA cm^{-2} as compared to an untreated MEA during continuous operation for 20 h [15]. Zhao et al. [16] systematically studied the effects of four different types of break-in protocols on the performance of a DMFC and determined that a break-in procedure involving operation of the cell under a H_2/O_2 mode yielded a positive impact on DMFC performance, although this benefit was manifested only in the mass transfer region of the polarization curve. Recently, Silva et al. [18] observed 2.5 times increase in DMFC power density, which is equivalent to the performance exhibited after conditioning the anode with hydrogen [19], under an in-situ break-in resulting from different operating conditions of DMFC. In nearly all of these studies, it has been suggested that the observed improvement in performance with the enhanced break-in protocol is most likely due to the opening of previously dead regions of the catalyst zone and creating beneficial structural changes to the catalytic zone, including changes in porosity, pore size, and connectivity between the electrolyte and catalyst particles due to rearrangement/swelling of the ionomer within the catalyst layer during the break-in operation of the cell [14,15,17].

While desirable structural changes can occur to the catalyst layer during break-in and initial stages of DMFC testing, the undesirable dissolution of Ru from PtRu anode is inevitable [8,20]. Ru dissolution becomes a serious issue particularly, when the anode potential exceeds 0.5 V, which is usually experienced during short-circuit events, fuel starvation, or occurrences of cell reversal during long-term DMFC operation [20–24]. In the context of Ru dissolution, electrochemical investigations of DMFC anodes are therefore usually restricted to below 0.8 V vs. DHE [25,26].

Interestingly, in recent years, some studies have revealed that treating the PtRu anode at a high anodic potential can significantly improved its performance [27–29]. Lu et al. [27] found that PtRu/C catalysts subjected to anodic treatment (AT) in 0.5 M H_2SO_4 with an upper potential limit of 1.3 V vs. RHE for 30 min promoted the MOR activity by nearly ~50%. This concept was subsequently applied in a real DMFC, yielding a 48% power density improvement after the PtRu black anode underwent AT at 0.7 V vs. RHE for 30 min [28]. A PtNiCr/C anode showed similar enhancement in MOR activity after AT in 0.5 M H_2SO_4 with an upper potential limit of 1.4 V [29]. These investigations suggested that the MOR activity is promoted by the electrochemical formation of reversible hydrous metal-oxide species, particularly by the formation of Ru hydrous oxide ($RuO_2 \cdot xH_2O$) at high anodic potential [30–33].

In the present work, both fresh and used MEAs containing a commercial PtRu/C (Hi-SPEC®) anode catalyst are subjected to AT at 0.8 V vs. DHE using potentiostatic mode for 80 h. The DMFC performance is significantly improved (by nearly 15%) after AT at 0.8 V for 80 h compared to the performance prior to AT. Performance improvements are also observed even after longer AT periods such as 120 h and 160 h as well. In order to understand the reasons for the performance improvement, XPS investigations are carried out for the PtRu/C catalyst, the anode of a decal-type MEA, and the anodes of MEAs with and without AT. Significant differences are observed in the metal content, composition of the Ru and Pt phases as well as carbon content of the catalyst and Nafion ionomer for the AT vs. non-AT MEAs. Furthermore, we observe changes in the distribution of Ru phases, i.e. progressive depletion of Ru oxides and enrichment in metallic Ru, in addition to reorganization of Nafion ionomer within the anode catalyst layer during AT. We hypothesize that the reorganization of Nafion ionomer in the anode catalyst layer may create a percolating network of ionomer between PtRu/C agglomerates, which helps to improve the utilization of PtRu for the MOR. This protocol can be adapted in addition to conventional break-in protocols and can also be used to rejuvenate old/used MEAs in order to improve long-term DMFC performance. These results, in concert with other recent literature reports [27–29] provide new insight into the treatment of PtRu-based DMFC anodes at high anodic potential in order to improve DMFC performance.

2. Experimental

2.1. MEA fabrication

In this study, we fabricated a total of six identical MEAs represented as MEA-1, MEA-2, MEA-3, MEA-4 (MEA-4 is an old MEA used for DMFC performance evaluation earlier and kept idle for almost a year), MEA-5-No-AT and MEA-6-AT. Details on the amount of AT treatment and other electrochemical tests applied to each of these 6 MEAs are provided in Table 1. In addition, a decal MEA was fabricated by coating only 30 wt.% PtRu/C on one side of a Nafion 117 membrane. The decal MEA was prepared exclusively for XPS studies as a reference for the initial composition of the anode prior to any electrochemical testing but after the catalyst is mixed with Nafion ionomer and the ink is sprayed on the membrane. All the MEAs were 5 cm^2 in area and were fabricated using a spray-coating method described elsewhere [34]. Briefly, catalyst inks for the anode and the cathode were prepared by mixing appropriate amounts of 30 wt.% PtRu/C (Hi-SPEC®) and 40 wt.% Pt/C (JM Hi-spec 4000), respectively, with isopropyl alcohol and ultrasonicated for 15 min. Then, 30 wt.% of Nafion solution was added to both the PtRu/C and Pt/C mixtures to make the anode and cathode inks, respectively and further ultrasonicated for 10 min. Subsequently, the prepared PtRu/C and Pt/C homogeneous catalyst inks were sprayed on either side of pretreated Nafion 117 membranes. The anode and cathode catalyst loadings were maintained to 2 mg cm^{-2} for both the anodes and cathodes of all the MEAs. Finally, the MEAs were hot pressed at a temperature of 135 °C under a load of 133 kg for 10 min.

Table 1
Details of AT and other electrochemical measurements for MEAs consisting of PtRu/C (Hi-spec 5000) anode.

MEAs	Cumulative AT time in h	Electrochemical measurements
Decal MEA	–	–
MEA-1	0, 80	DMFC performance, MOR in anode, CO stripping in anode, LT DMFC for 50 h (done after AT)
MEA-2	0, 160 (80 + 40 + 40)	DMFC performance, MOR in anode, CO stripping in anode
MEA-3	0, 80	DMFC performance, MOR in anode, CO stripping in anode, LT DMFC for 50 h (done prior to AT)
MEA-4 (old/used MEA)	0, 160 (80 + 80)	DMFC performance, MOR in anode, CO stripping in anode, LT DMFC for 50 h (done after AT-80 h), LT MOR in anode
MEA-5	0	DMFC performance, MOR in anode
MEA-6	0, 80	DMFC performance (prior to AT)

2.2. DMFC testing

To test DMFC performance, the MEAs were assembled in single-cell test fixtures by placing microporous carbon coated carbon paper, which acted as a gas diffusion layer (GDL), on either side of the MEAs. Serpentine-type graphite separators with channel dimensions of 1 mm × 1 mm (depth × width) were employed. After assembling the MEAs, preconditioning was carried out by a two-step process involving hydrogen–air testing prior to methanol–air conditioning [13]. Initially, the cell was preconditioned by discharging at 0.6 V for 2 h by feeding humidified H_2 (105 ml min^{-1}) and air (350 ml min^{-1}) to the anode and cathode, respectively, at 80 °C. The cell voltage was then maintained at 0.6 V for 10 min and 0.8 V for 5 min and this discharging cycle was repeated for 20 h. In the subsequent step, the cell was discharged at a constant current of 0.1 A using 0.5 M methanol (2 ml min^{-1}) and humidified air (200 ml min^{-1}) at 80 °C for 6 h. After preconditioning, initial DMFC performance curves were obtained by feeding 1 M methanol (2 ml min^{-1}) and humidified air (200 ml min^{-1}) to the anode and cathode, respectively, at ambient pressure and at 80 °C. The DMFC performance testing was carried out galvanostatically by increasing the current in 15 min steps and the corresponding voltage values were recorded with a commercial test station (Teledyne Energy Systems, Inc., USA). The voltage values recorded for the last 5 min at each current step were averaged and used for plotting the polarization curves. The long-term durability test was carried out by discharging the cell at constant cell voltage of 0.4 V using 1 M methanol (2 ml min^{-1}) and humidified air (200 ml min^{-1}) to the anode and cathode, respectively, at ambient pressure and at 80 °C for a period of 50 h.

2.3. AT for anode of the MEAs

AT for the MEA anodes was conducted at 0.8 V vs. DHE for 80, 120 and 160 h using a potentiostat (Solartron Analytical, Model 1470E, USA). The AT protocol involved feeding the anode (which served as the working electrode) with humidified N_2 (100 ml min^{-1}), while the cathode (which acted as the counter and reference electrode) was fed with humidified H_2 (100 ml min^{-1}). Initially, the anode potential was swept up to 0.8 V vs. DHE by LSV at a scan rate of 25 mV s^{-1}. Subsequently, the anode potential was maintained at 0.8 V during the entirety of the anodic treatment at ambient pressure and at a temperature of 30 °C. After AT for 80 h, detailed electrochemical measurements including CO stripping voltammetry and linear sweep voltammetry (LSV) were acquired using a potentiostat (Solartron Analytical, Model 1470E, USA).

2.4. Electrochemical characterization of the MEAs

CO stripping voltammetry was used to determine the ECSA of the anode and cathode at the initial condition and to assess changes to the anode and cathode after AT at 0.8 V. To perform CO stripping for the anode, high-purity humidified 0.1% CO in argon (200 ml min^{-1}) and H_2 (100 ml min^{-1}) were fed to anode and cathode, respectively. For the cathode CO stripping, the respective gases were switched, i.e. 0.1% CO in argon (200 ml min^{-1}) and H_2 (100 ml min^{-1}) were fed to the cathode and anode, respectively. For each stripping experiment, 0.1% CO in argon was fed to the electrode of interest (anode/cathode) while its potential was maintained at 0.1 V for 30 min. Then, humidified N_2 (200 ml min^{-1}) was fed to the electrode for another 30 min while still maintaining the potential at 0.1 V. Subsequently, the CO stripping curves were collected in the potential region from 0.05 to 0.9 V at a scan rate of 5 mV s^{-1} at 25 °C under a back pressure of 14.7 psi.

Activity of the anode was determined from the MOR polarization curves before and after AT at 0.8 V vs. DHE. The MOR polarization curves were collected using LSV by feeding 1 M methanol (2 ml min^{-1}) and hydrogen (100 ml min^{-1}) to the anode and cathode, respectively, in the potential region from 0 to 0.7 V at a scan rate of 5 mV s^{-1} at 80 °C. Chronoamperometric MOR activity was also measured for 180 min before and after 80 h AT at 0.5 V vs. DHE under the same conditions mentioned above.

2.5. XPS characterization

XPS survey and high-resolution spectra were acquired on a Kratos Nova X-ray photoelectron spectrometer with a monochromatic Al K source that was operated at 300 W. Pass energies were 160 eV for the survey spectra and 20 eV for the high-resolution spectra of C 1s/Ru 3d, O 1s, N 1s, F 1s, Ru 3p, and Pt 4f. In addition to the full data sets acquired for each sample with a minimum of two areas per sample, multiple scans were also acquired from C 1s/Ru 3d region to check reproducibility of the composition in various areas on the MEAs (Fig. S4 in the Supplementary data). Data processing was performed using Casa XPS software and involved background subtraction, charge calibration, and curve-fitting. A linear background was applied to C 1s/Ru 3d, O 1s, N 1s and F 1s regions, while Shirley background was used for Pt 4f and Ru 3p regions. Charge referencing was done to the carbon peak at 284.8 eV. Due to interference of C 1s and Ru 3d peaks, elemental quantification of ruthenium species was performed using the Ru 3p region. The distribution of Ru species was evaluated from the Ru 3d region, which was analyzed using consistent fitting parameters and constraints for all analyzed areas/samples. Ru 3d was fitted with 3 peaks, each containing $3d_{5/2}$ and $3d_{3/2}$ components separated by 4.2 eV as shown in Fig. 7 and Table 5. The $3d_{5/2}$ component of the first doublet is located at 280.6 eV, which is due to the presence of metallic ruthenium. The $3d_{5/2}$ components of the second and third doublets are due to ruthenium oxide present in both the anhydrous and hydrous forms with respective binding energies of 281.5 and 282.5 eV [35–38]. It is most likely that the first C 1s peak, located at 283.7 eV, also has a small contribution from Ru species that are typically reported at 283.5 eV and assigned either to ruthenium oxide in a higher oxidation state or unscreened final state [35,36]. In order to systematically investigate changes in the composition of PtRu/C in the anode, XPS was performed on the following materials: as received PtRu/C catalyst powder, anode of the decal MEA, MEA-1, MEA-3, MEA-5-No-AT, and MEA-6-AT (AT and testing history details of MEAs are given in Table 1).

3. Results and discussion

3.1. DMFC performance of the MEAs

Fig. 1 compares the DMFC performance of two identical MEAs (MEA-1 and MEA-2) before AT vs. after AT for 80 h (1a), the improvement in DMFC performance of MEA-2 after 80, 120 and 160 h AT (1b), and the % improvement of maximum power density as a function of AT for MEA-2 (1c). Both MEAs exhibit a higher OCV and improved performance throughout all current density regions after undergoing AT. After 80 h AT, MEA-1 and MEA-2 yield maximum power densities of 125 and 122 mW cm^{-2} vs. initial maximum power densities of 110 and 106 mW cm^{-2} before AT (Fig. 1a). A similar performance trend is observed even after AT for 120 and 160 h. For instance, MEA-2 attains maximum power densities of 119 and 123 mW cm^{-2} after AT for 120 and 160 h representing improvements of 13–15% in the maximum power density (Fig. 1b and c). Interestingly, we have observed similar if not larger DMFC performance improvements (18% improvement or more) for MEAs made of in-house synthesized PtRu supported on either un-

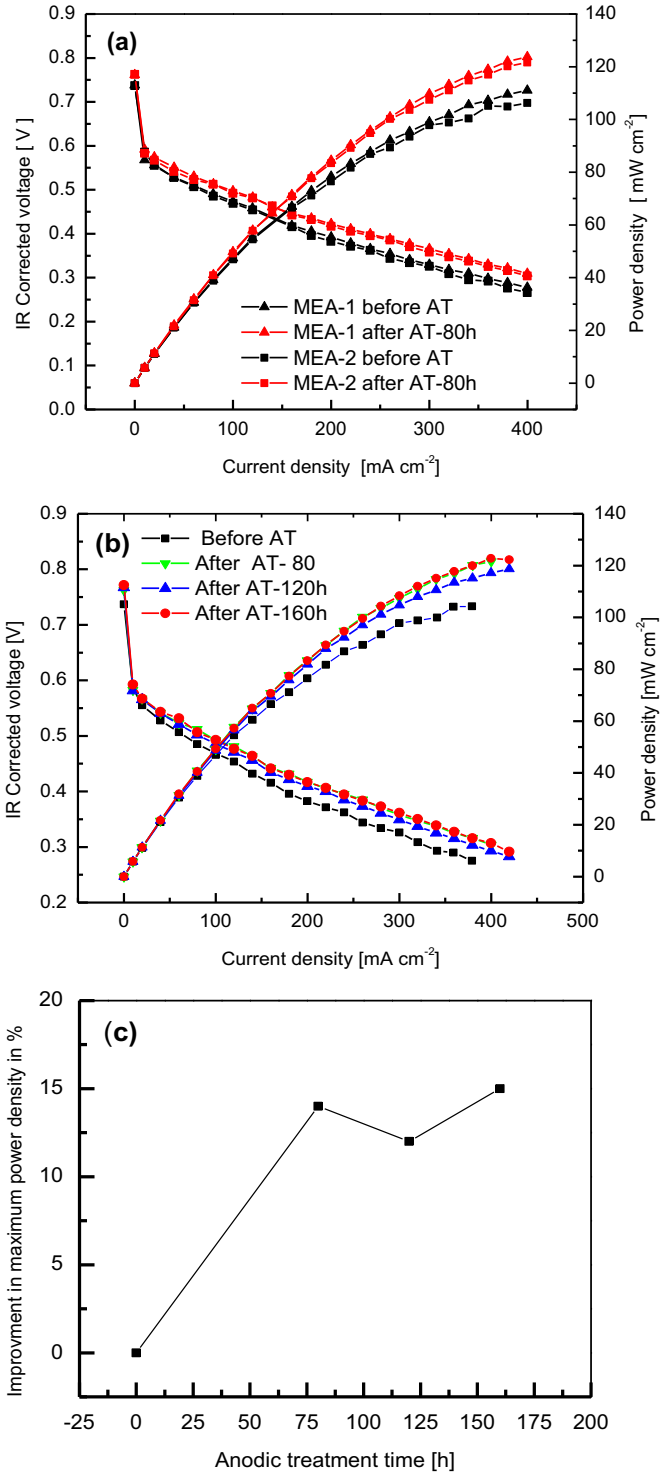

Fig. 1. (a) Comparison of DMFC performance of MEA-1 and MEA-2 before and after AT for 80 h; (b) DMFC Performance of MEA-2 after the anode was subjected to AT for 80 h, 120 h and 160 h and; (c) % improvement in power density as a function of AT time for MEA-2.

doped or N-doped carbon [20]. The cell and anode performance data along with ECSA for the anodes of MEA-1 and MEA-2 are summarized in Table 2. Since the improvement in performance after 80, 120, and 160 h AT appears to be more or less equivalent, the following electrochemical and XPS investigations are mainly focused on the MEAs that were subjected to AT for 80 h.

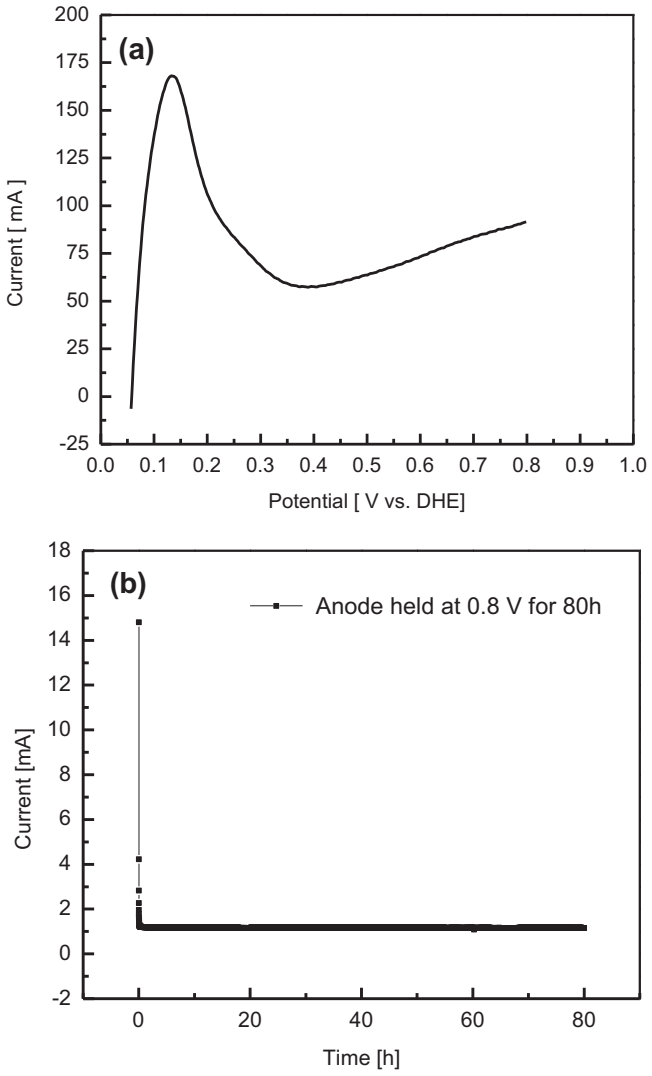

Fig. 2. (a) LSV curve for the anode of the MEA-2 swept up to 0.8 V vs. DHE and; (b) Anode of the MEA-2 held at 0.8 V for 80 h.

3.2. AT for MEAs

Fig. 2 shows the LSV curve for the anode of MEA-2 swept up to 0.8 V (scan rate of 25 mV s^{-1}), after which the anode was held at the potential of 0.8 V for 80 h for the purpose of AT. As can be seen in Fig. 2a, the anode current gradually increases as the potential is swept above 0.4 V and it attains a peak transient value of 87 mA at 0.8 V, likely indicating the preferential formation of Ru higher oxides [20,27,28]. When the anode potential is maintained at 0.8 V for 80 h for the AT, the current rapidly decreases to ~1.1 mA after only a few minutes as shown in Fig. 2b, and this value is then maintained during the entire 80 h AT period. Although the reason for the large drop in current from the initial value of 87 to ~1.1 mA at 0.8 V is not clearly understood, it is believed to be mainly due to continuation of Ru dissolution during AT. The reorganization of ionomer takes place in the catalyst layer (will be discussed by the XPS analysis in the later part) is not expected to contribute for the observed small current. The total coulombs of charge passed during the anodic treatment is calculated by integrating the chronoamperometric current vs. time curve and is found to be 3946 C after AT for 80 h. The observed value of 3946 C for 80 h is significantly lower than the value of 8578 C reported by Lai et al. [22] for a PtRu black anode that underwent AT

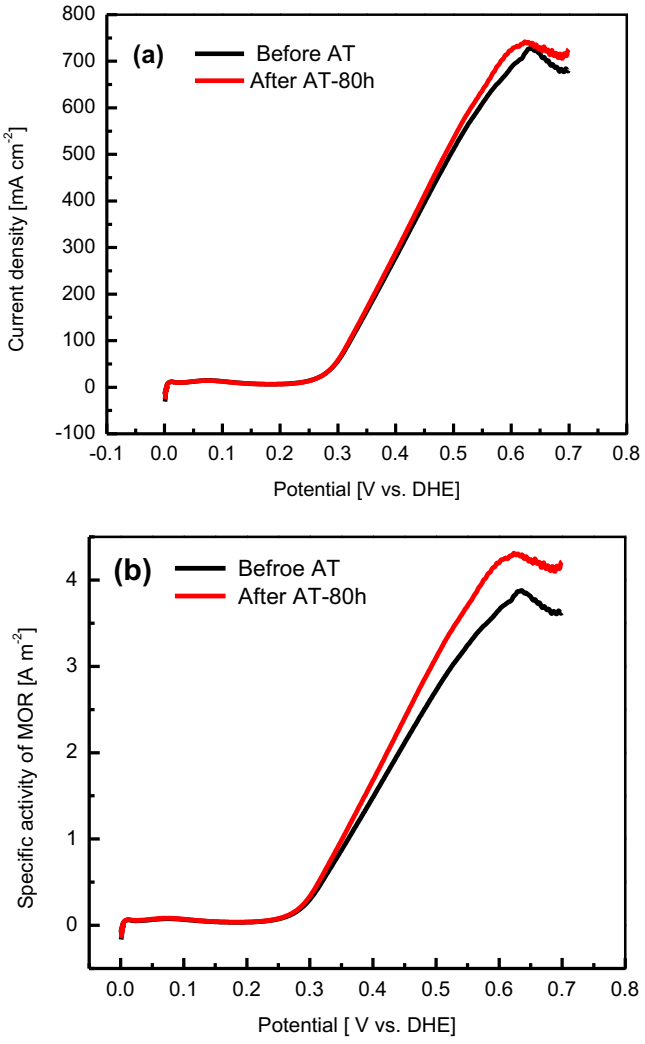

Fig. 3. MOR polarization curves for anode of the MEA-1 before and after AT for 80 h (a) Raw data for the MOR and; (b) MOR current normalized by ECSA.

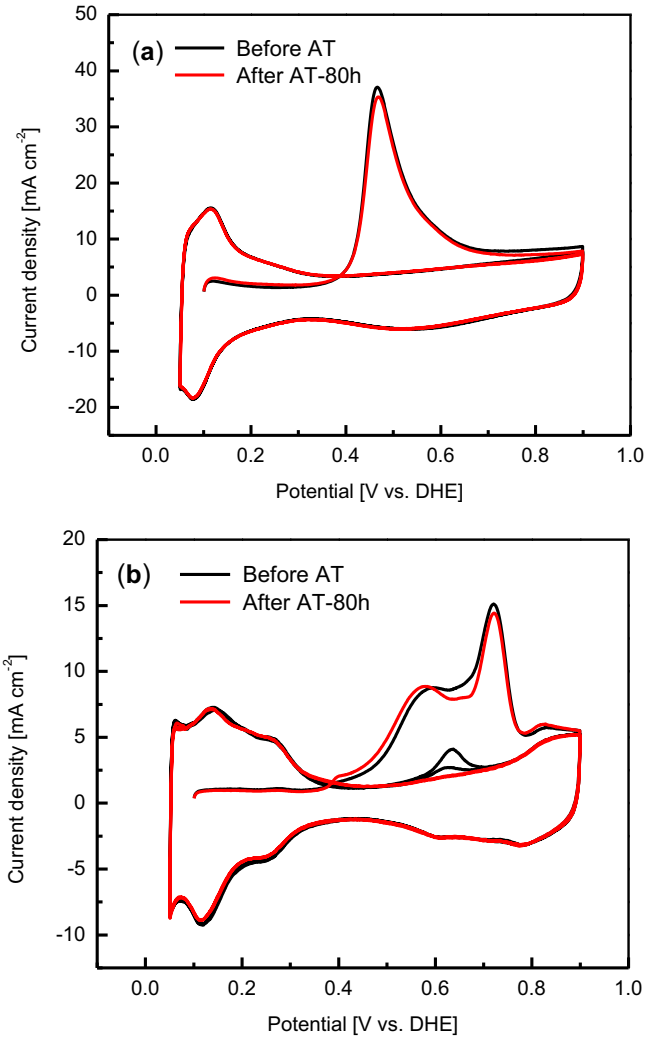

Fig. 4. CO stripping voltammograms for the anode and cathode of MEA-1 (a) CO stripping voltammogram for the anode before and after AT for 80 h and; (b) CO stripping voltammogram for the cathode before and after AT for 80 h.

at 0.8 V for 80 h under conditions similar to those used in this study. In that study, severe Ru dissolution was observed (consistent with the higher coulomb value) that led to a marked degradation in the cell performance [22]. The lower amount of charge observed in this study might be interpreted as a reduction in Ru dissolution during AT at 0.8 V for 80 h. However, XPS analysis (discussed later), does show that the AT protocol conducted in this study results in at least some loss of ruthenium, and also causes changes in the distribution of ruthenium species toward metallic ruthenium.

3.3. MOR polarization curves

In order to further probe the phenomenon of improved DMFC performance during AT, the MOR activity of the anode of MEA-1 was assessed via LSV after 80 h AT under the same operating conditions used for DMFC performance testing (Fig. 3). The MOR current density increases slightly after AT in the high potential region (e.g. 550 mA cm^{-2} vs. 510 mA cm^{-2} at 0.5 V vs. DHE, Fig. 3a). The improvement in MOR current density in the higher anodic potential region after AT is consistent with the DMFC polarization data, which shows significant performance improvement in the ohmic and mass transfer regions. On the other hand, the MOR current density in the lower potential region (0.28–0.4 V) remains almost equivalent before vs. after AT and the MOR onset potential does not change. This is most likely due to dissolution of Ru or RuO_2 after AT (discussed in the CO stripping data for anode of the MEAs in the following section), which usually does not allow the MOR onset potential to take place on the negative side [39,40]. A similar type of MOR behavior is also observed for the MEA-2 (figure not shown) and the MOR current density values for MEA-1 and MEA-2 at 0.5 V are given in Table 2. The dissolution of Ru or RuO_2 leads to loss in ECSA, which is taken into account in calculating the specific activity of the MOR (MOR intrinsic catalytic activity) by normalizing the current by the measured anode ECSA after AT for the MEA-1 and MEA-2 as shown in Fig. 3b and in Fig. S1 in the Supplementary data, respectively. This analysis reveals that the specific activity of the MOR is significantly improved at 0.5 V for both the MEAs after AT. The MOR mass and specific activity values for MEA-1, MEA-2 and MEA-4 (which will be discussed in the later section) at 0.5 V are given in Table 3.

3.4. CO stripping voltammetry

Fig. 4 shows the anode and cathode CO stripping voltammograms for MEA-1 prior to AT and after 80 h AT. Before AT the anode CO oxidation peak is a single, narrow with a potential at 0.47 V;

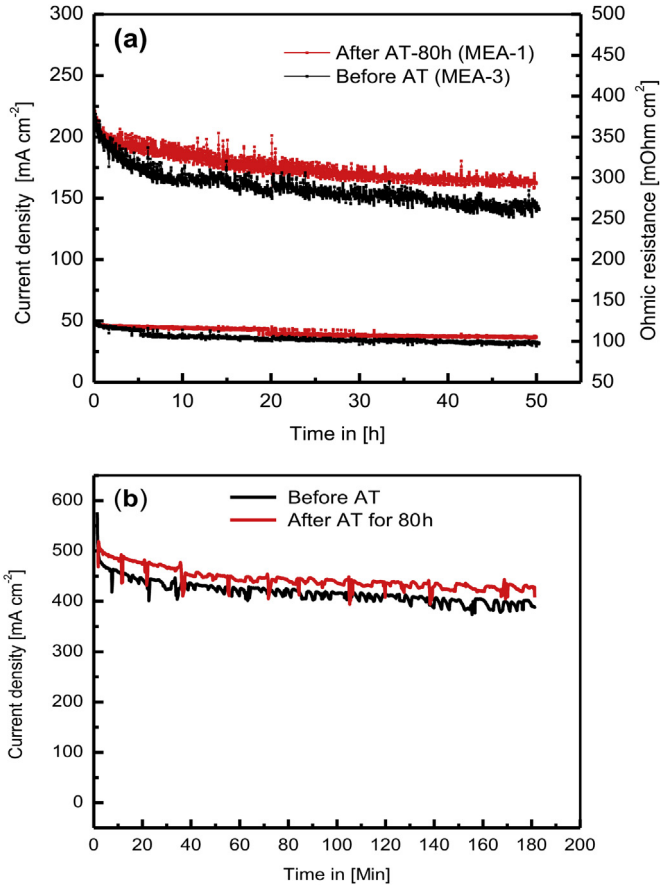

Fig. 5. (a) Comparison of long-term DMFC performance of MEA-1 (after AT for 80 h) and MEA-3 (Before AT) carried out at constant voltage of 0.4 V and; (b) Comparison of long-term MOR activity for the anode of MEA-4 (Before and after AT for 80 h) carried out at constant potential of 0.5 V vs. DHE for 180 min.

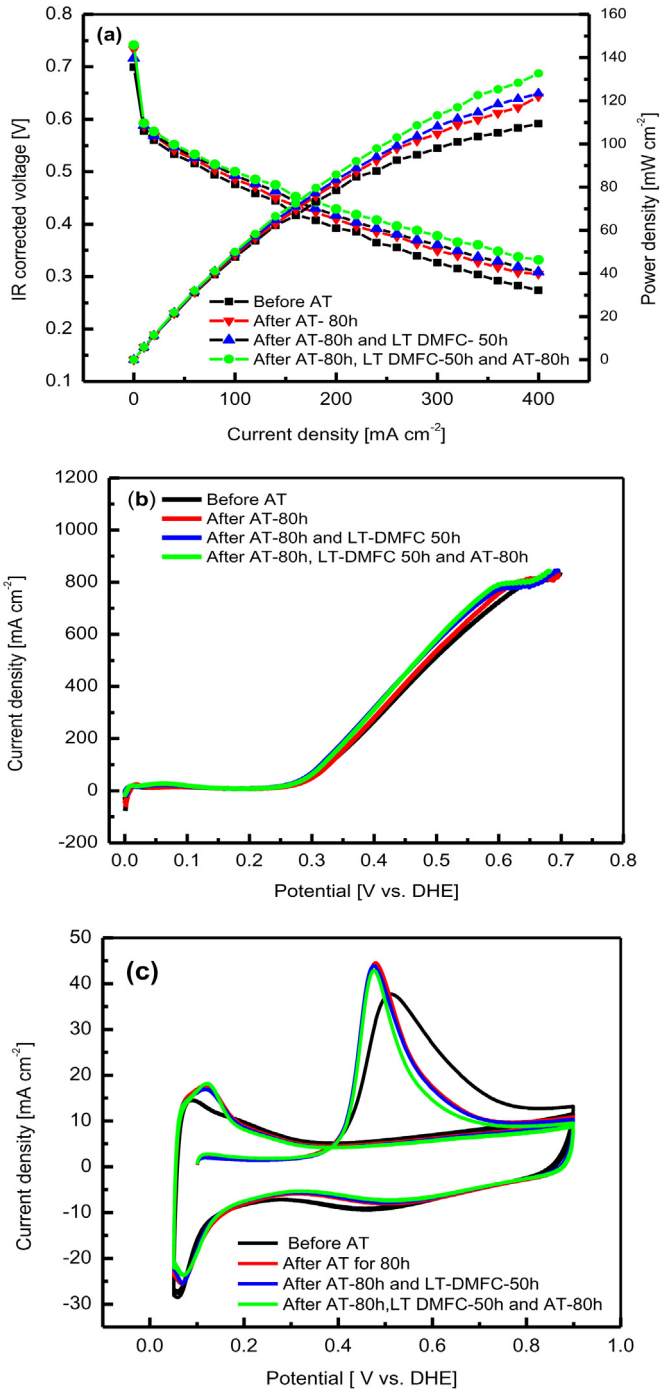

Fig. 6. (a) DMFC performance of MEA-4; (b) MOR polarization curves for the anode of MEA-4; and (c) CO stripping voltammogram for the anode of MEA-4.

after AT, the peak occurs at an identical potential, but with slightly reduced current density (Fig. 4a). This indicates a slight decrease of the anode ECSA after AT. The decrease in anode ECSA was also observed for MEA-2 after AT for 80 h (Fig. S2 in the Supplementary data). The calculated ECSA values for the anodes of MEA-1 and MEA-2 are given in Table 3. The decrease in ECSA can be attributed to the dissolution of either Ru metal or RuO_2 from the anode during AT, which is confirmed by the CO stripping results for the cathode (40 wt.% Pt/C) of MEA-1 as shown in Fig. 4b. Even prior to AT, the cathode stripping curve shows a significant CO oxidation peak at 0.60 V in addition to the primary CO oxidation peak associated with Pt at ~0.73 V [10]. The observed peak at 0.60 V suggests that Ru species are already present on cathode of the MEA even during the initial performance testing [41]. This observation is well supported by XPS analysis (discussed later) that confirms ruthenium loss from the anode occurs not only during initial performance, but also during decal MEA fabrication and preconditioning, where Ru crossover to the cathode is also detected.

The observed decrease in anode ECSA after AT is somewhat contradictory to the improvement in DMFC performance, but it can perhaps be attributed to the difference in the mechanism of CO oxidation (a gas/solid process) vs. methanol oxidation (a liquid/solid process) on PtRu/C [41]. The loss of Ru from the anode leads to a reduction in ECSA because Ru has a higher tendency to adsorb CO and its loss thereby reduces the charge of the CO oxidation peak to some extent. However, reorganization of Nafion ionomer leads to improvement of catalyst–ionomer interactions that occur mainly due to decreased concentration of hydrophobic CF_2 groups in the anode catalyst layer (the details will be discussed in the XPS section below), which mostly benefit the MOR process, and not the CO oxidation process. This benefit outweighs the ECSA losses and leads to the improvement in DMFC performance despite the ECSA loss [41].

3.5. Long-term DMFC performance

Fig. 5 compares the long-term DMFC performance of MEA-1 (after 80 h AT) vs. MEA-3 (prior to AT) at constant voltage 0.4 V

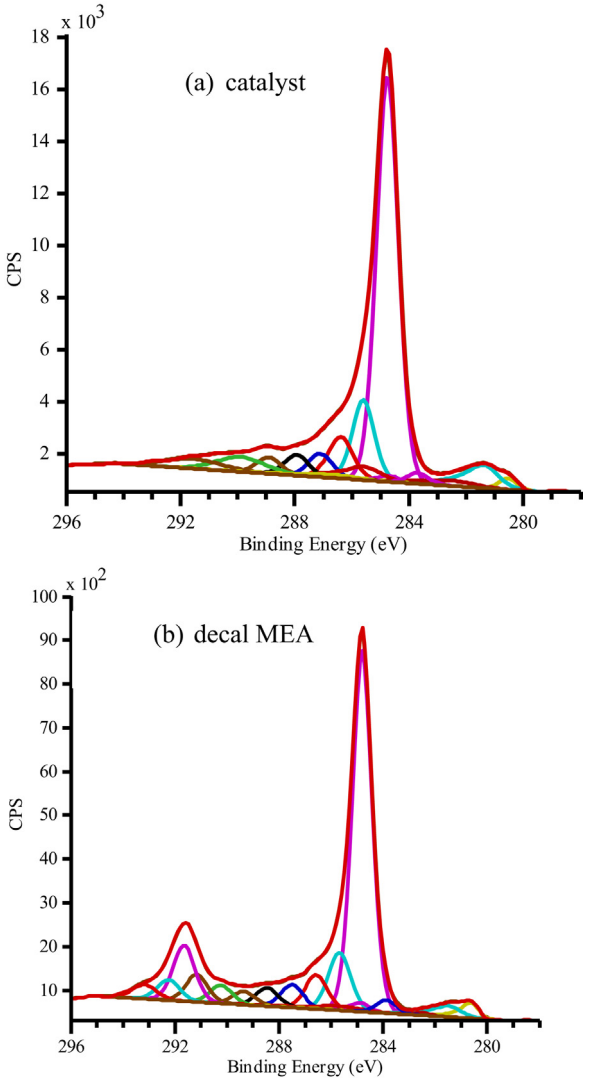

Fig. 7. High resolution C 1s + Ru 3d spectra, curve-fitted (a) PtRu/Carbon catalyst; and (b) PtRu/Carbon decal MEA.

for 50 h under the same performance operating conditions. As DMFC MEAs generally undergo severe performance loss during the initial stages of long-term operation [12,42], it is interesting to compare the endurance of the MEA subjected to AT-80 h vs. the untreated MEA during the first 50 h of durability testing. Both MEAs exhibit identical initial current density values of 225 mA cm^{-2} at 0.4 V. As shown in Fig. 5a, MEA-3 experiences faster performance degradation than MEA-1 during the initial 10 h of testing. The performance of both MEAs subsequently degrade at a similar rate and the current densities gradually decline to 170 and 140 mA cm^{-2}, respectively, at the end of 50 h. Overall, MEA-1 shows significantly reduced performance degradation (by ~12%) as compared to MEA-3. This smaller performance degradation is observed despite the fact that MEA-1 shows a slightly higher ohmic resistance than MEA-3 (which might have been caused by migrated ruthenium at the cathode interface of MEA-1 after AT). Here, it should be mentioned that the initial performances of MEA-1 and MEA-3 are almost identical to each other (figure not shown).

DMFC performance degradation during the initial stage of long-term testing is mainly attributed to PtO_x formation in the cathode, cathode depolarization effects caused by methanol crossover, and the non-equilibrium state of ruthenium oxide and its involvement in the oxidation of CH_3OH and its intermediate species in the anode [12,42–44]. Although many of these factors might be similar for both the MEAs, it is hypothesized that the depolarization effect caused by methanol crossover in the cathode is minimized in MEA-1 because of the higher efficiency of the MOR facilitated by the reorganization of Nafion ionomer in the catalyst layer after AT. In order to verify the higher efficiency of methanol oxidation in the anode subjected to AT, we have carried out long-term methanol oxidation on the anode of MEA-4 before and after AT for 80 h at 0.5 V vs. DHE by feeding H_2 to the cathode for 180 min (Fig. 5b). As can be seen in the figure, the initial decay in methanol oxidation current (which is mainly attributed to the formation of intermediate species, such as CH_3OH_{ads}, CO_{ads} and CHO_{ads} [45]) is significantly reduced after AT 80 h as compared to before AT. Moreover, after AT the anode maintains a higher methanol oxidation current density (by ~13%) over the entire period as compared to the same anode prior to AT.

3.6. Performance rejuvenation of used MEAs

So far, we have discussed the improvements in initial and long-term DMFC performance for fresh MEAs subjected to AT at 0.8 V vs. DHE. In this section, we demonstrate how AT can also help rejuvenate the DMFC performance of a used MEA (used for initial performance test and stored idle for a year before carrying out the tests mentioned below). Fig. 6 shows the DMFC performance curves (6a), MOR activity in the anode (6b) and anode CO stripping curves (6c) measured for MEA-4 before AT, after 80 h AT, after long-term DMFC testing for 50 h, and then after a second 80 h AT period.

Table 2
Cell performance and MOR activity for MEA-1 and MEA-2 before and after AT for 80 h.

MEAs	AT time in h	OCV in volts	Peak power density in mW cm^{-2}	Current density of MOR at 0.5 V vs. DHE (mA cm^{-2})
MEA-1	0	0.741	110	510
	80	0.753	125	550
MEA-2	0	0.740	106	600
	80	0.752	122	595

Table 3
MOR mass activity, MOR specific activity and anode ECSA for MEA-1, MEA-2 and MEA-4 before and after AT for 80 h.

MEAs	AT time in h	Mass activity of the MOR at 0.5 V vs. DHE (A g^{-1})	ECSA of anode (m^2 g^{-1})	Specific activity of the MOR at 0.5 V vs. DHE (A m^{-2})
MEA-1	0	267	93.9	2.70
	80	278	86.1	3.20
MEA-2	0	258	126.6	2.25
	80	270	116.0	2.50
MEA-4	0	268	149.6	1.80
	80	280	128.8	2.24

Table 4
Cell performance, MOR activity and anode ECSA of MEA-4 before and after AT for different periods.

MEA	Cumulative AT time in h	OCV in volts	Peak power density in mW cm^{-2}	Current density of MOR at 0.5 V (mA cm^{-2})	ECSA of anode (m^2 g^{-1})
MEA-4	0	0.690	110	520	149.6
	80	0.720	120	565	128.8
	160	0.740	132	602	113.7

Table 5
XPS elemental composition, at.%.

Elemental composition (at.%)						
Sample	Catalyst	Decal MEA	MEA-5, no AT	MEA-6, after AT	MEA-1, final	MEA-3, final
Carbon, C 1s	91.1	70.0	70.6	74.9	76.3	75.3
Oxygen, O 1s	6.2	4.8	3.2	2.7	3.0	3.4
Fluorine, F 1s	0.0	23.8	25.2	21.4	19.5	20.2
Platinum, Pt 4f	1.36	0.69	0.46	0.52	0.61	0.55
Ruthenium, Ru 3p	1.32	0.76	0.51	0.47	0.62	0.62
C/F	–	2.9	2.8	3.5	3.9	3.7
Pt + Ru	2.7	1.4	1.0	1.0	1.2	1.2
Pt/Ru	1.0	0.9	0.9	1.1	1.0	0.9

Initially, MEA-4 shows an OCV value of 0.690 V and delivers a maximum power density of 110 mW cm^{-2}. After subsequent AT for 80 h, the OCV and performance are improved, particularly in the ohmic and in the mass transfer regions. Then, after carrying out the long-term DMFC test at a constant potential of 0.4 V for 50 h (the long-term performance data is almost similar to that of MEA-1 and is shown in Fig. S3 in the Supplementary data), the performance actually improves again slightly (the long-term test for 50 h is therefore not a long enough to cause a degradation in the cell performance). Moreover, as discussed earlier, the performance benefits provided by subjecting the MEA to AT prior to the 50 h DMFC test may help to maintain stability. When an additional 80 h of AT is then provided to the anode, significant further improvement is observed in the OCV (0.747 V) and in the cell performance (132 mW cm^{-2}). Overall, the performance of MEA-4 improves by nearly 17% after the 50 h of long-term testing sandwiched by the two 80 h AT periods.

3.7. MOR polarization for used MEAs

The MOR activity for the anode of MEA-4 was measured under the same operating conditions used for the cell performance test (Fig. 6b). The observed cell performance trends are reflected in the MOR activity of the anode after each testing interval. Similar to the observations from MEA-1 (Fig. 3), no big changes are found in the MOR onset potential before vs. after the first 80 h AT, after long-term DMFC testing for 50 h, or after the second 80 h AT. However, in the high potential region (0.5 V), the MOR current density increases incrementally after each of the two AT periods. The MOR specific activity of MEA-4 is measured by normalizing the current by anode ECSA after AT for 80 h and is given in Table 3. The improvement in the OCV, cell and anode performance data of MEA-4 before and after the different periods of AT are given in Table 4.

3.8. CO stripping voltammetry for used MEAs

CO stripping voltammograms for the anode of MEA-4 were carried out before initial DMFC performance testing, after the first 80 h AT period, after the 50 h long-term DMFC test, and after the second 80 h AT period (Fig. 6c). Initially, a broader CO oxidation peak is observed for this used MEA (in contrast to the narrow peak observed for the fresh MEAs) with a peak potential of 0.52 V and a maximum current density of 35 mA cm^{-2}. After DMFC performance testing followed by AT for 80 h, the CO oxidation peak narrows significantly and the peak potential shifts negatively by nearly ~60 mV (0.46 V), while the maximum current density of the peak increases to 45 mA cm^{-2}. After the subsequent long-term DMFC performance testing for 50 h, the CO oxidation peak potential and the area under the peak remain almost unchanged. These observations are consistent with the DMFC performance data. The CO oxidation peak measured after the final 80 h AT further narrows, while the area under peak is slightly reduced, which is most likely due to further Ru dissolution as discussed earlier in the context of the AT of the other MEAs. The ECSA values calculated from the CO stripping curves are given in Table 4. The observed initial broad peak is most likely due to the presence of greater amounts of Ru oxide species, which are speculated to be formed on PtRu during the year-long storage period for this MEA prior to the present testing. The presence of Ru oxides is confirmed by the formation of a small hydrogen desorption peak in the potential region 0.05–0.15 V and a slight negative shift in the Ru oxides reduction peak as compared with the base voltammogram curves (see Fig. 6c) [27]. These Ru oxides are likely reduced to Ru when methanol is fed to the anode during the initial DMFC performance tests as reported in the literature [46] and also observed from our CO stripping data for the anode of MEA made of in-house PtRu/C. This is substantiated by the fact that the CO oxidation peak becomes narrower and shifts negatively after AT, indicating that Ru is now mostly present in its metallic state. The XPS investigations (figure not shown) reveal that MEA-4 has the lowest concentration of ruthenium with all three types of ruthenium species being significantly depleted. The higher

Table 6
Quantification of deconvoluted XPS spectra of C 1s and Ru 3d, relative concentration, at.%.

Quantification of C 1s + Ru 3d, relative concentration, %							
	Catalyst		Decal MEA	MEA-5, no AT	MEA-6, after AT	MEA-1, final	MEA-3, final
Ru, (Ru1–Ru6)	0.77	Ru, (Ru1–Ru6)	0.42	0.29	0.28	0.33	0.32
C1, 283.7 eV	1.7	C1, 283.8 eV	1.9	1.7	1.4	1.5	1.6
C2, 284.8 eV	59.1	C2, 284.8 eV	51.9	53.3	56.0	56.8	56.3
C3, 285.6 eV	13.6	C3, 285.7 eV	8.8	8.0	7.4	9.0	7.8
C4, 286.4 eV	7.0	C4, 286.4 eV	5.3	5.2	5.0	5.1	5.1
C5, 287.1 eV	3.9	C5, 287.3 eV	3.7	4.0	4.1	3.7	4.4
C6, 287.9 eV	3.0	C6, 288.3 eV	3.0	3.0	3.3	2.6	3.1
C7, 288.9 eV	2.4	C7, 289.3 eV	2.6	2.5	2.6	2.9	2.7
C8, 289.9 eV	4.3	C8, 290.3 eV	3.0	2.6	2.6	2.9	2.4
C9, 291.6 eV	4.2	C9, 291.1 eV	4.2	2.5	3.3	4.6	3.2
		C10, 291.7 eV	9.3	6.7	4.0	4.8	5.2
		C11, 292.4 eV	3.3	8.2	8.0	4.4	6.1
		C12, 293.3 ev	2.6	2.1	2.1	1.5	1.9
	86.6	Cs, (C2–C6)	72.7	73.5	75.9	77.1	76.6
		Ci, (C9–C12)	19.4	19.5	17.3	15.2	16.4
		Cs/Ci, C2–C6/C9–C12	3.7	3.8	4.4	5.1	4.7
	113.2	C2–C6/Ru	175	258	276	234	243
		C9–C12/Ru	47	68	63	46	52

total Ru dissolution sustained by this MEA is consistent with its long usage and storage history and longer cumulative AT (160 h AT in total).

3.9. Compositional analysis by XPS

In this section, in order to substantiate the reasons behind the significant improvement in DMFC performance caused by the AT protocol, we detail the extensive XPS analyses conducted for the as-received PtRu catalyst powder, a decal MEA anode (that was never subjected to any electrochemical testing) as well as most of the tested MEAs (some of which received AT and some of which did not). Table 5 summarizes the elemental composition for each of these samples. The PtRu/C powder sample contains catalyst platinum and ruthenium species and carbon associated with carbon support, while the rest of the samples (the decal MEA anode and the other MEA anodes) also contain Nafion ionomer. Incorporation of Nafion ionomer into the catalytic layer results in the presence of ~20–25% fluorine and the appearance of several new carbon functionalities at BE 291–293 eV, corresponding to the various C–F bonds present in the Nafion ionomer [47–50]. As a result of the Nafion ionomer addition, the relative amounts of catalyst (platinum and ruthenium) and carbon decrease. Detailed analyses of the combined regions of C 1s and Ru 3d for the PtRu/C powder and the decal MEA anode are shown in Fig. 7a and b, while Tables 5 and 6 summarize the quantification of these regions for all analyzed samples. To facilitate comparative analysis of the quantified combined C 1s and Ru 3d region, Table 5 reports the sum of carbon peaks C1 through C6 corresponding to C=C, C–C, C–H, C–O and C=O functionalities, all of which are associated with the support (Cs), and the sum of carbon peaks C9 through C12 corresponding to CFO, CF_2 and CF_3 functionalities, which are associated with the ionomer (Ci) [49]. Table 6 also presents the Cs/Ci ratio which is expected to follow the same trend as the elemental C/F composition ratio reported in Table 5. Ratios of Cs/Ru and Ci/Ru are used to elucidate whether the decrease in ruthenium signal is only associated with the addition of the Nafion ionomer or if there is also a decrease in the amount of Ru relative to the carbon support.

By comparing the C 1s spectra from PtRu/C powder and the decal MEA anode normalized to the peak maximum at 284.8 eV as shown in Fig. 8a, it is clear that the major difference between the two is the appearance of carbon peaks associated with the ionomer, which include peaks due to CF–O at 291.1 eV, CF_2 at 291.7, CF_2–O at 292.4 and CF_3 at 293.3 eV. It is also evident that relative amount of ruthenium vs. support carbon is decreased (Table 6). This indicates that the decrease in the ruthenium signal is associated with ruthenium dissolution, as discussed above (CO stripping voltammetry in Fig. 4), not just because of the Nafion addition.

A more detailed understanding of the changes in the catalyst composition can be derived by analyzing the distribution of ruthenium species (Table 7) and by comparing the Pt 4f spectra for the PtRu/C powder vs. the decal MEA anode (Fig. 9a). Not surprisingly, the initial catalyst contains substantial amounts of oxidized species [51,52]. In the decal MEA, however, the catalyst is more enriched with metallic components, as both the anhydrous and hydrous ruthenium oxides and platinum oxides are depleted.

The differences in the anode composition for MEA-5 vs. MEA-6 (no AT vs. AT) follow somewhat different trends. The decrease in platinum and ruthenium content (Tables 5 and 6) are accompanied by depletion of anhydrous and hydrous ruthenium oxides (Fig. 8b and c and Table 7) and only very small changes in the distribution of platinum species (Fig. 9b and c). This indicates even further enrichment of metallic ruthenium in the catalyst layers for both MEAs compared to the decal MEA anode. However, the fluorine content for the two MEAs are quite different from the decal MEA, with MEA-6-AT having the lowest amount of fluorine and MEA-5-No-AT having the highest fluorine concentration of the three samples (Tables 5 and 6). The changes in the amount of fluorine are also accompanied by redistribution of the relative amounts of carbon–fluorine functionalities (Fig. 8b and c). The amount of CF_2–O groups (associated with the hydrophilic side of the Nafion ionomer chain) increase in both MEAs compared to the decal anode. However, the amount of CF_2 groups (associated with hydrophobic side of the ionomer) is lower in MEA-6-AT than in the decal MEA or in MEA-5-No-AT. The depletion of Nafion ionomer and specifically, the hydrophobic CF_2 groups in the anode catalyst layer of the MEA

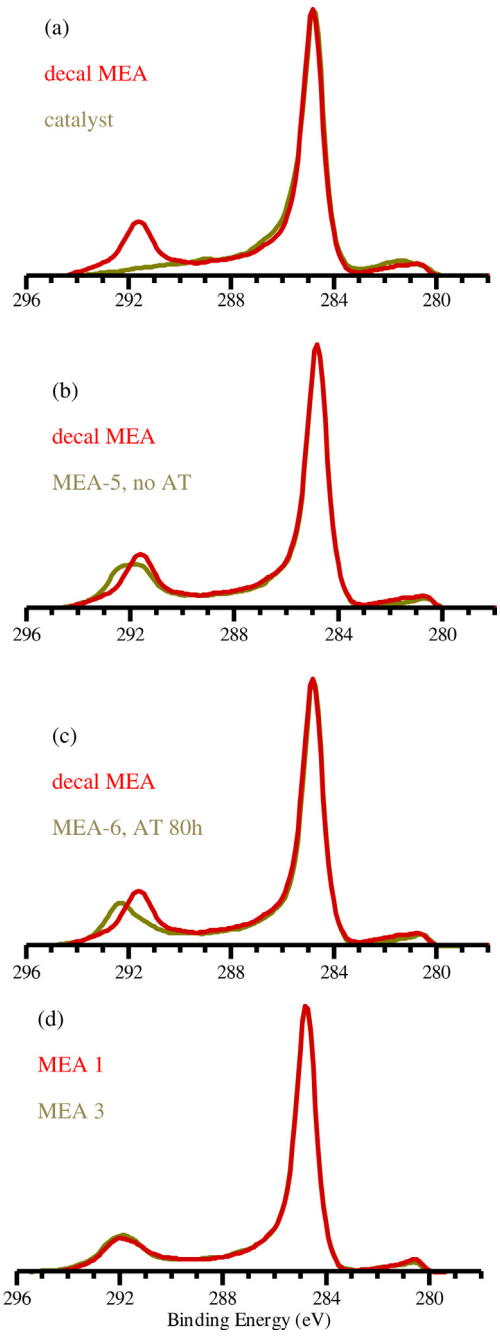

Fig. 8. Overlays of high resolution C 1s + Ru 3d spectra, normalized at the peak maximum for (a) decal MEA and catalyst; (b) decal MEA and MEA-5 with no AT; (c) decal and MEA-6 after 80 h AT; (d) MEA-1 and MEA-3, both are after AT and various performance tests.

Table 7
Quantification of deconvoluted XPS spectra of Ru 3d, relative concentration, %.

Quantification of Ru 3d, relative concentration, %						
Sample	Catalyst	Decal MEA	MEA-5, no AT	MEA-6, after AT	MEA 1, final	MEA 3, final
Ru metallic: Ru1 (280.6 eV) and Ru4 (284.8 eV)	13.9	44.1	60.9	73.9	68.1	62.8
RuO_2: Ru2 (281.5 eV) and Ru5 (285.7 eV)	59.4	49.4	30.9	26.1	29.5	30.2
$RuO_2 \cdot nH_2O$ (or RuO_xH_y) Ru3 (282.5 eV) and Ru6 (286.7 eV)	26.7	6.5	8.2	0.0	2.5	7.0

subjected to AT might be an indication of reorganization of the ionomer on the surface of the anode catalyst layer.

It appears that the distribution of Ru species (shown in Table 7 and Fig. 8d) and the distribution of Pt species (not shown) in the two other AT-treated MEAs (MEA-1 and MEA-3), which underwent extensive electrochemical testing (see Table 1) in the preceding sections of the paper are quite similar to each other. Similar to MEA-6, these two additional AT-tested MEAs also have lower fluorine concentration and lower amounts of hydrophobic CF_2 groups. The slightly higher relative concentrations of platinum and ruthenium observed for these samples might be related to the lower fluorine amount on the surface. The lower amount of F and hydrophobic CF_2 groups is again possibly indicative of reorganization of the Nafion ionomer.

Some of the literature reports suggest that the formation of Ru hydrous oxide ($RuO_2 \cdot xH_2O$) species could be a reason for the improvement in DMFC performance after subjecting the anode to a high potential treatment in 0.5 or 1.0 M H_2SO_4 solution [27–29]. In our study, when comparing the composition of anodes subjected to AT (in presence of humidified N_2) vs. those without AT, we have not detected any increment in the amount of $RuO_2 \cdot xH_2O$ species. We find that hydrous ruthenium oxide species are largely decreased after AT. It is possible that when the MEA is in a non-hydrated state, some of the hydrous ruthenium oxide species convert into non-hydrous forms and therefore are not detected during XPS analysis. However, according to XPS analysis, the amount of non-hydrous ruthenium oxide is also decreased in the catalyst. From the literature reports [27–29] and our study, it is understood that the oxidation state of PtRu particularly, Ru differs to a greater extent when it is fed with H_2SO_4 solution vs. humidified N_2 under bias at high potential. The H_2SO_4 solution possibly penetrates deep into the catalyst layer and is more likely to accelerate the oxidation of Ru compared with the humidified N_2. Therefore, based on our XPS results, we hypothesize that the improvement in the DMFC performance after AT using humidified N_2 should instead most likely be related to changes in the catalyst–ionomer interface. Reorientation of the Nafion ionomer can potentially generate a more continuous percolating network of ionomer between PtRu/C agglomerate (by the possible incorporation of Nafion ionomer within the secondary pores of the PtRu/C agglomerates) [53,54], which would in turn help to improve the utilization of the PtRu/C catalyst for the MOR. In addition, our XPS results suggest an increase the hydrophilic character of the ionomer after AT. The schematic representation of Nafion reorganization in the anode catalyst layer and the resultant improvement in the hydrophilic character of the Nafion ionomer after AT is depicted in Fig. 10. The improvement in hydrophilic character of the Nafion ionomer could result in improved accessibility for the methanol fuel, which leads to improvement in performance, particularly in the ohmic and mass transfer regions as discussed in Fig. 3.

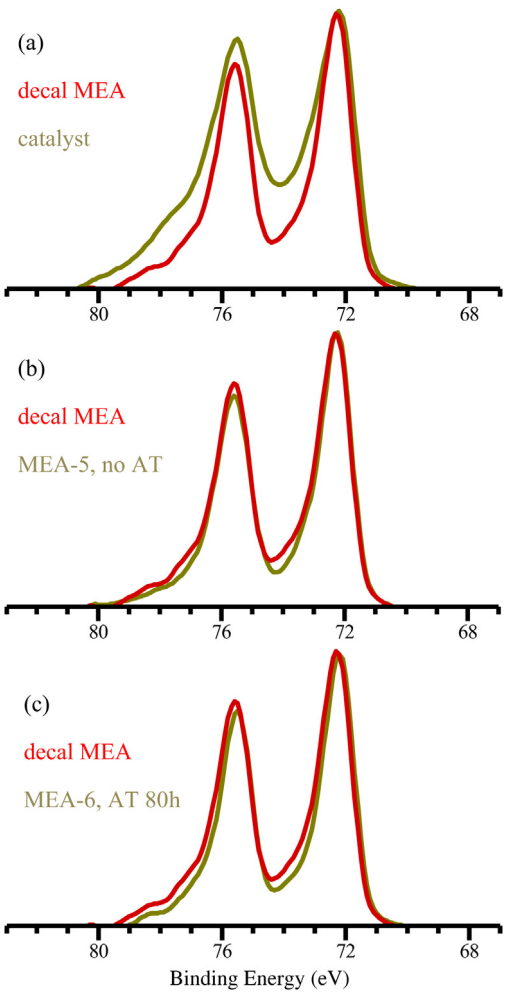

Fig. 9. Overlays of high resolution Pt 4f spectra, normalized at the peak maximum for (a) decal MEA and catalyst; (b) decal MEA and MEA-5 with no AT; and (c) decal MEA and MEA-6 after AT 80 h.

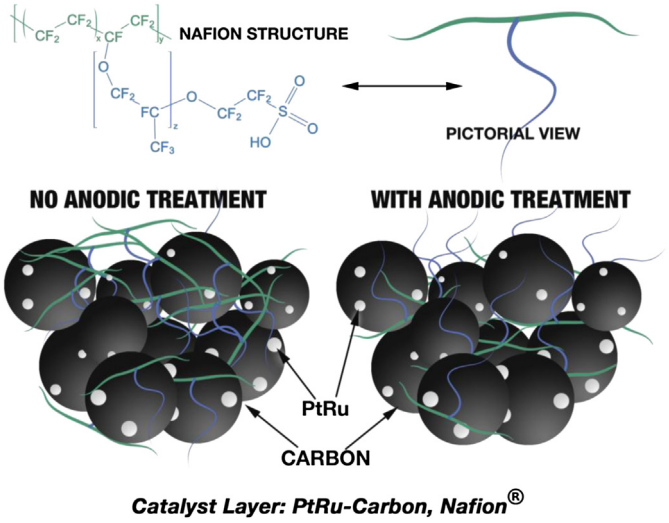

Fig. 10. Schematic representation of Nafion ionomer reorganization in the anode catalyst layer after AT.

4. Conclusion

A significant improvement in DMFC performance is observed in the ohmic and mass transfer regions for MEAs fabricated from a commercial PtRu/C catalyst (Hi-SPEC®) that are subjected to an anodic-treatment protocol at 0.8 V vs. DHE. This performance improvement (~15% improvement in max power density) occurs despite the fact that there is a slight decrease in the anode ECSA. In addition, MEAs subjected to AT show significantly reduced performance degradation during a 50 h constant potential performance test. XPS results suggest that the improvement in the performance of the MEAs subjected to AT might be correlated to reorganization of the Nafion ionomer within the anode catalyst layer, as evidenced from a decrease in the amount of ionomer and a decrease in the amount of hydrophobic CF_2 surface groups after AT. There are at least two potential beneficial aspects of this ionomer reorganization: 1) it may enable further incorporation of Nafion within the secondary pores of PtRu/C agglomerates in the catalyst layer, thereby improving the percolating network of Nafion ionomer between PtRu/C agglomerates and 2) the enhancement of the hydrophilic character of the ionomer may increase the accessibility of methanol in the anode catalyst layer, thereby resulting in performance improvement in the ohmic and mass transfer regions. The protocol suggested in this work can be adapted in addition to conventional break-in protocols, and can also be used to rejuvenate the anodes of old MEAs in order to improve DMFC performance. However, further work should be aimed at minimizing/optimizing the AT time, which would increase the ease of this new break-in protocol for practical applications.

Acknowledgments

This work was supported by the Army Research Office under grant #W911NF-09-1-0528 and the U.S. Department of Energy EERE, Fuel Cell Technologies Program, under Contract No. DE-AC36-08-GO28308 with the National Renewable Energy Laboratory. The authors also acknowledge surface analysis and fuel cell testing facilities provided at NREL.

Appendix A. Supplementary data

Supplementary data related to this article can be found at http://dx.doi.org/10.1016/j.jpowsour.2013.06.105.

References

[1] B. McNicol, D.A.J. Rand, K.R. Williams, J. Power Sources 83 (1999) 15–31.
[2] K. Scot, W.M. Taama, J. Power Sources 79 (1999) 43–59.
[3] P. Liu, G.-P. Yin, C.-Y. Du, Electrochem. Commun. 10 (2008) 1471–1473.
[4] H. Liu, C. Song, L. Zhang, J. Zhang, H. Wang, D.P. Wilkinson, J. Power Sources 155 (2006) 95–110.
[5] N. Munichandraiah, K. McGrath, P.G.K. Surya, R. Aniszfeld, G.A. Olah, J. Power Sources 117 (2003) 98–101.
[6] B. Gurau, E.S. Smotkin, J. Power Sources 112 (2002) 339–352.
[7] J. Prabhuram, T.S. Zhao, H. Yang, J. Electroanal. Chem. 578 (2005) 105–112.
[8] P. Piela, C. Eickes, E. Brosha, F. Garzon, P. Zelenay, J. Electrochem. Soc. 151 (2) (2004) A2053–A2059.
[9] L. Liu, L. Zhang, X. Cheng, Y. Zhang, ECS Trans. 19 (23) (2009) 43–51.
[10] J.-H. Choi, Y.S. Kim, R. Bashyam, P. Zelenay, ECS Trans. 1 (8) (2006) 437–445.
[11] J. Liu, Z. Zhou, X. Zhao, Q. Xin, G. Sun, B. Yi, Phys. Chem. Chem. Phys. 6 (2004) 134–137.
[12] J. Prabhuram, N.N. Krishnan, B. Choi, T.-H. Lim, H.Y. Ha, S.-K. Kim, Int. J. Hydrogen Energy 35 (2010) 6924–6933.
[13] M. Inoue, T. Iwasaki, K. Sayama, M. Umeda, J. Power Sources 195 (2010) 5986–5989.
[14] C. He, Z. Qi, M. Hollett, A. Kaufman, Electrochem. Solid-State Lett. 5 (8) (2002) A181–A183.
[15] B.-K. Kho, I.-H. Oh, S.-A. Hong, H.Y. Ha, Fuel Cells Bull. (2004) 11–14.
[16] X. Zhao, W. Lei, A. Manthiram, J. Power Sources 201 (2012) 37–42.
[17] G. Liu, J. Xu, T. Wang, T. Zhao, M. Wang, Y. Wang, J. Li, X. Wang, Int. J. Hydrogen Energy 35 (2010) 12341–12345.
[18] V.B. Silva, A. Rouboa, Fuel 93 (2012) 677–683.
[19] H.N. Dinh, X. Ren, F.H. Garzon, P. Zelenay, S. Gottesfeld, J. Electroanal. Chem. 491 (2000) 222–233.
[20] J. Prabhuram, S. Pylypenko, T.S. Olson, A. Dameron, A. Corpuz, K. Wood, K. O'Neill, K. Hurst, G. Bender, H.N. Dinh, T. Gennett, B. Pivovar, R. O'Hayre, J. Electrochem. Soc. 159 (11) (2012) F768–F778.
[21] E. Antolini, J. Solid State Electrochem 15 (2011) 455–472.
[22] C.-M. Lai, J.-C. Lin, K.-L. Hsueh, C.-P. Hwang, K.-C. Tsay, L.-D. Tsai, Y.-M. Peng, J. Electrochem. Soc. 155 (8) (2008) B843–B851.
[23] S.H. Jordanov, H.A. Kozlowsska, M. Vukoviff, B.E. Conway, J. Electrochem. Soc. 125 (1978) 1471–1480.
[24] W. Chen, G. Sun, Z. Liang, Q. Mao, H. Li, G. Wang, Q. Xin, H. Chang, C. Pak, D. Seung, J. Power Sources 160 (2006) 933–939.
[25] B. Beden, F. Kadirgan, C. Lamy, J.M. Leger, J. Electroanal. Chem. 127 (1981) 75–85.
[26] C.L. Green, A.J. Kucernak, J. Phys. Chem. B 106 (2002) 1036–1047.
[27] Q. Lu, B. Yang, L. Zhuang, J. Lu, J. Phys. Chem. B 109 (2005) 1715–1722.
[28] M.K. Jeon, J.Y. Won, S.I. Woo, Electrochem. Solid-State Lett. 10 (1) (2007) B23–B25.
[29] M.K. Jeon, P.J. McGinn, J. Power Sources 188 (2009) 427–432.
[30] D.R. Rolison, P.L. Hagans, K.E. Swider, J.W. Long, Langmuir 15 (1999) 774–779.
[31] J.W. Long, R.M. Stroud, K.E.S. Lyons, D.R. Rolison, J. Phys. Chem. B 104 (2000) 9772–9776.
[32] F. Scheiba, M. Scholz, L. Cao, R. Schafranek, C. Roth, C. Cremers, X. Qiu, U. Stimming, H. Fuess, Fuel Cells 06 (2006) 439–446.
[33] S. Trasatti, Electrochim. Acta 36 (1991) 225–241.
[34] J.H. Cho, J.M. Kim, J. Prabhuram, S.Y. Hwang, D.J. Ahn, H.Y. Ha, S.-K. Kim, J. Power Sources 187 (2009) 378–386.
[35] S. Pylypenko, A. Queen, T.S. Olson, A. Dameron, K. O'Neill, K.C. Neyerlin, B. Pivovar, H.N. Dinh, D.S. Ginley, T. Gennett, R. O'Hayre, J. Phys. Chem. C 115 (2011) 13676–13684.
[36] S. Pylypenko, B.B. Blizanac, T.S. Olson, D. Konopka, P. Atanassove, Appl. Mater. Interfaces 1 (2009) 604–611.
[37] H. Kim, I.R.D. Moraes, G.T. Filho, R. Haasch, A. Wieckowski, Surf. Sci. 474 (2001) L203–L212.
[38] A. Lewera, W.P. Zhou, C. Vericat, J.H. Chung, R. Hassch, A. Wieckowski, P.S. Bagus, Electrochim. Acta 51 (2006) 3950–3956.
[39] J.-F. Drillet, H. Bueb, R. Dittmeyer, U.D. Weglikowska, S. Roth, J. Electrochem. Soc. 156 (10) (2009) F137–F144.
[40] M.P. Hogarth, G.A. Hards, Platinum Met. Rev. 40 (1996) 150–159.
[41] H.A. Gasteiger, N. Markovic, P.N. Ross Jr., E.J. Cairns, J. Phys. Chem. 98 (1994) 617–625.
[42] J.-Y. Park, M.A. Scibioh, S.-K. Kim, H.-J. Kim, I.-H. Oh, T.G. Lee, H.Y. Ha, Int. J. Hydrogen Energy 34 (2009) 2043–2051.
[43] H. Hoster, T. Iwasita, H. Baumgartner, W. Vielstich, J. Electrochem. Soc. 148 (2001) A496–A501.
[44] H. Hoster, T. Iwasita, H. Baumgartner, W. Vielstich, Phys. Chem. Chem. Phys. 3 (2001) 337–346.
[45] J.W. Guo, T.S. Zhao, J. Prabhuram, R. Chen, C.W. Wong, J. Power Sources 156 (2006) 345–354.
[46] F. Liu, C.-Y. Wang, Electrochim. Acta 50 (2005) 1413–1422.
[47] K. More, DOE Annual Merit Review, Fuel Cells and Hydrogen Technology Division, 2011.
[48] K. Artyushikova, D.H. Rodriguez, T.S. Olson, P. Atanassov, J. Power Sources 226 (2013) 112–121.
[49] G.B.D. Beamson, The Scienta ESCA300 Database, Wiley, Chichester, 1992, p. 295.
[50] C. Chen, G. Levitin, D.W. Hess, T.F. Fuller, J. Power Sources 169 (2007) 288–297.
[51] J.B. Goodenough, A. Hamnett, B.J. Kennedy, R. Manoharan, S.A. Weeks, J. Electroanal. Chem. 240 (1988) 133–145.
[52] A. Hamnett, B.J. Kennedy, Electrochim. Acta 33 (1988) 1613–1618.
[53] M. Uchida, Y. Aoyama, N. Eda, A. Ohta, J. Electrochem. Soc. 142 (1995) 4143–4149.
[54] E. Passalacua, F. Lufrano, G. Squadrito, A. Patti, L. Giorgi, Electrochim. Acta 46 (2001) 799–805.